Optimal trapping stability of *Escherichia coli* in oscillating optical tweezers

Amarjeet Yadav,[1,*] Anindita Dutta,[1,*] Pramod Kumar,[1,2] Yuval Dahan,[1] Alexander Aranovich,[1] and Mario Feingold[1]
[1]*Department of Physics and The Ilse Katz Center for Nanotechnology, Ben Gurion University of the Negev, Beer Sheva 84105, Israel*
[2]*Department of Physics, Institute of Nanotechnology and Advanced Materials, Bar-Ilan University, Ramat Gan 52900, Israel*

(Received 28 February 2019; revised manuscript received 27 March 2020; accepted 7 April 2020; published 1 June 2020)

Single-beam oscillating optical tweezers can be used to trap rod-shaped bacterial cells and align them with their long axis lying within the focal plane. While such configuration is useful for imaging applications, the corresponding imaging resolution is limited by the fluctuations of the trapped cell. We study the fluctuations of four of the coordinates of the trapped cell, two for its center of mass position and two for its angular orientation, showing the way they depend on the trap length and the trapping beam power. We find that optimal trapping stability is obtained when the trap length is about the same as the cell length and that cell fluctuations in the focal plane decrease like the inverse of the trapping power.

DOI: 10.1103/PhysRevE.101.062402

I. INTRODUCTION

Optical tweezers (OT) have been widely used in single-cell studies either for measuring their various biomechanical properties [1–3] or, alternatively, for cell manipulation, sorting and microsurgery [4–8]. Recently, it was shown that optical trapping may also be useful for single-cell imaging [9–12]. Individual trapped cells can be immobilized while embedded in fluid medium. This approach avoids the potential optical difficulties that may result from the presence of a solid substrate, e.g., agarose, to which the cell adheres. Moreover, optical traps can be used to properly orient cells such as to obtain an optimized perspective on the particular subcellular structure that is to be imaged [13,14]. Trapped cells can be rapidly reoriented to image either different cellular components or the same one from different viewpoints.

A significant fraction of the single-cell studies involving the use of optical traps were done on rod-shaped bacteria and mainly on the Gram-negative *Escherichia coli* [12,15,16]. This is both due to their simple geometry and their being among the simplest living organisms. In most of the OT bacterial imaging studies, trapped *E. coli* cells were oriented either with their long axis in the (x,y) focal plane, horizontal orientation, or with their long axis perpendicular to the focal plane, vertical orientation. Since the trapping force of standard single-beam OT is stronger in the (x,y) plane than in the perpendicular direction, z, the trap aligns elongated objects, including rod-shaped bacteria, along the z axis. Traditionally however, rod-shaped bacteria have been imaged in the horizontal orientation while cells are attached to a hydrogel pad. For this reason, a significant effort was made to image rod-shaped bacteria that are both trapped and horizontally aligned.

Several optical trapping methods have been used to horizontally orient rod-shaped bacteria [12–14,17–19]. The simplest approach consists of using dual traps whereby each of the two traps holds the cell at one of its ends [12,17,18]. Recently, the nucleoids of individual *E. coli* cells were imaged by direct stochastic optical reconstruction microscopy (*d*STORM) together with a dual OT system [12]. Since *d*STORM requires a relatively long acquisition time, ∼90 s, the random fluctuations of the trapped cell significantly lower the imaging resolution. To bypass this problem, Diekmann *et al.* used the fluctuations distribution of the trapped cell to deconvolute the resulting *d*STORM image leading to a resolution that was below 100 nm. Nevertheless, the extent of the fluctuations of the trapped cell represents the main limiting factor that prevents reaching a resolution of around 30 nm as for *d*STORM imaging of immobile cells. Therefore, further improving the stability of the trapped cell will allow obtaining higher resolution in imaging setups of this type.

Another OT configuration that was used to trap bacilli in a horizontal orientation is the tug-of-war (TOW) tweezers [19]. It consists of a dual linear trap that stretches the trapped cell exerting opposite forces on each of its two ends. To obtain the appropriate beam shape, the system includes a spatial light modulator (SLM) along the optical path that encodes holographic information. Bezryadina *et al.* [19] have used TOW tweezers to study the mechanical properties of biofilms measuring the force required to break up aggregates of several bacterial cells. Moreover, they have compared the trapping stability of TOW tweezers and dual traps suggesting that the former are more stable. First, they showed that while the fluctuation distribution of the trapped cell for the dual trap is the same in the x (along the cell) and y (perpendicular to the cell) directions, for the TOW tweezers the distributions in the x and y directions are very different from each other. Specifically, the TOW distribution in y is thinner and that in x is wider than the corresponding distributions in the dual trap. It appears that while the two-dimensional fluctuation distribution of the trapped cell is elongated in the x direction for the TOW tweezers, its area is similar to that of the distribution obtained in the case of the dual trap. Consequently, the overall imaging resolution of trapped cells in TOW tweezers

[*]These authors contributed equally to this work.

and dual traps is likely to be similar, although the different resolutions in the x and y directions in the case of the TOW tweezers represent a significant limitation. Second, trapping stability was characterized in an oscillating flow of varying amplitude and frequency. Mapping the escape threshold in each of the x, y, and z directions, it was shown that for TOW tweezers cells remain trapped at higher amplitudes for each particular frequency than in equivalent dual traps. However, the escape amplitude threshold represents a measure of the overall trapping force, a property of traps not directly relevant to the imaging of immobilized cells.

In recent years, we have introduced another approach to horizontally align rod-shaped bacteria that is simpler than the TOW tweezers and relatively flexible [13,14]. We use a single trap that oscillates at a sufficiently high frequency to effectively generate a linear trap. The length of the linear trap is determined by the amplitude of the oscillation. Oscillating traps that are slightly longer than the cell length were found to display optimal horizontal trapping stability. We have used such oscillating traps to image individual *E. coli* cells in either phase contrast or fluorescence modes [20–22]. In what follows, we analyze the stability of trapping in oscillating tweezers to find the optimal parameters, namely, the oscillation amplitude and trapping power. Unlike in previous studies, we include angular fluctuations in addition to those of the center of mass in our analysis of cell trapping stability. We find that the trap length for which *E. coli* are most stably aligned in the oscillating tweezers is approximately equal to the cell length. Moreover, the variances of each of the coordinates that were studied are to a good approximation proportional to the inverse of the trapping beam power.

II. EXPERIMENTAL METHODS

A. Optical system

We have described our optical setup in detail in previous publications [13,14,21]. Here we will only present a brief summary. The system consists of an inverted microscope (IX70, Olympus), a cooled CCD (CoolSNAP ES^2, Photometrics), a near infrared diode laser (SDL, $\lambda = 830$ nm), and a galvanometric mirror (Cambridge Technology). The Gaussian laser beam is deflected by the galvanometric mirror and focused by the microscope objective lens (UPLFLN 100XO2PH, 1.3 NA, oil immersion) to obtain the trap. This objective is also used to image the trapped cells. A telescope is placed along the optical path allowing to adjust the height of the trap such that trapped cells lay in the focal plane. It is also used to expand the laser beam to overfill the back aperture of the objective. It consists of two plano-convex lenses, L_1 with a focal length, f_1, of 200 mm (Thorlabs), and L_2 with $f_2 = 130$ mm (Melles-Griot), located at a distance $f_1 + f_2$ from each other. The galvanometric mirror, the telescope and the objective back aperture lay in conjugate planes ensuring that the center of the trap remains in the focal plane throughout its oscillating trajectory.

In most of our experiments, the linear trap was obtained oscillating the galvanometric mirror sinusoidally at 100 Hz. For comparison, we also used other waveforms, e.g., square, sawtooth, etc. For high enough frequencies, square wave oscillating tweezers are essentially equivalent to double traps [Fig. 1(d)]. Cells were imaged in phase contrast and the pixel size was 41 nm. The sample chamber consists of a parafilm spacer (∼0.13 mm thickness) between two #1 round cover slips (22 mm diameter, Marienfeld). While the power of the trapping laser beam, P, as measured on top of the lower cover slip, was varied in the range between 4 and 11 mW, in experiments performed at constant power, we used $P = 9.65$ mW. The corresponding extent of heating due to the trapping beam is expected to be below 1°C. This aspect was extensively studied for silica and polystyrene microbeads trapped in nonoscillating tweezers showing that the heating occurs mostly via the fluid surrounding the trap [23]. Although our system is different from that of Ref. [23], the 1°C estimate is a safe upper bound on the heating of the trapped cell. Such small degree of heating will have a negligible effect on the stability of trapping for rod-shaped cells.

B. Calibration of the galvanometric mirror

To calibrate the oscillating tweezers, we image the time averaged intensity distribution of the laser beam, $I(x,y)$, in the focal plane [Figs. 1(c) and 1(d)]. To this end, we focus the beam on the bottom of the sample (upper surface of the bottom coverslip) and use an exposure time of 20 ms, twice the oscillation period. For the sinusoidal oscillation, the $I(x,y)$ distribution has a stadium-like shape with maxima at its ends [Figs. 1(a) and 1(c)]. We define the length of the trap, L_{trap}, as the sum of the distance between the two maxima of $I(x,y)$, D, and the full width at half maximum (FWHM) of the nonoscillating laser beam intensity profile [Fig. 1(b)], d, $L_{\text{trap}} = D + d$. For the square wave case, the trap length can be defined in the same way, although here, $I(x,y)$ consists practically of two Gaussian distributions with FWHM $= d$ located at a distance D of each other along the x direction [Fig. 1(d)], as long as D is larger than $\sim 2d$. The FWHM of the nonoscillating laser beam in the focal plane, d, is obtained from a quantitative analysis of the corresponding image (not shown). In particular, we measure the intensity profile along an axis passing through the center of the beam image. After subtracting the background and normalizing the maximal intensity to 1, we fit a Gaussian distribution to the resulting intensity [Fig. 1(b)]. We find that the FWHM of the best fitting Gaussian is 1.10 ± 0.01 μm and define it to be the width of the nonoscillating optical trap, d.

In our system, we control L_{trap} via the oscillation amplitude of the galvanometric mirror. Specifically, in the range of amplitudes used in our experiment, the distance between the two maxima of $I(x,y)$, D, depends linearly on the root-mean square (RMS) of the oscillating voltage, V_{rms} [Figs. 1(e) and 1(f)]. The best linear fit to the measured values of D, $D = aV_{\text{rms}} + b$, corresponds to $a = 0.243 \pm 0.003\,\mu$m/mV and $b = -0.8 \pm 0.1\,\mu$m for the sinusoidal case [Fig. 1(e)] and $a = 0.174 \pm 0.001\,\mu$m/mV and $b = -0.09 \pm 0.04\,\mu$m for the square wave voltage [Fig. 1(f)]. This calibration together with the value of d allows us to determine the length of the trap, L_{trap}, for the two waveforms at different RMS voltages, V_{rms}. We note that the intercept, b, of the linear fit to the $D(V_{\text{rms}})$ does not vanish, mainly in the case of the sinusoidal oscillation. In part, this is due to D being slightly smaller than the beam oscillation amplitude. However, the main reason is

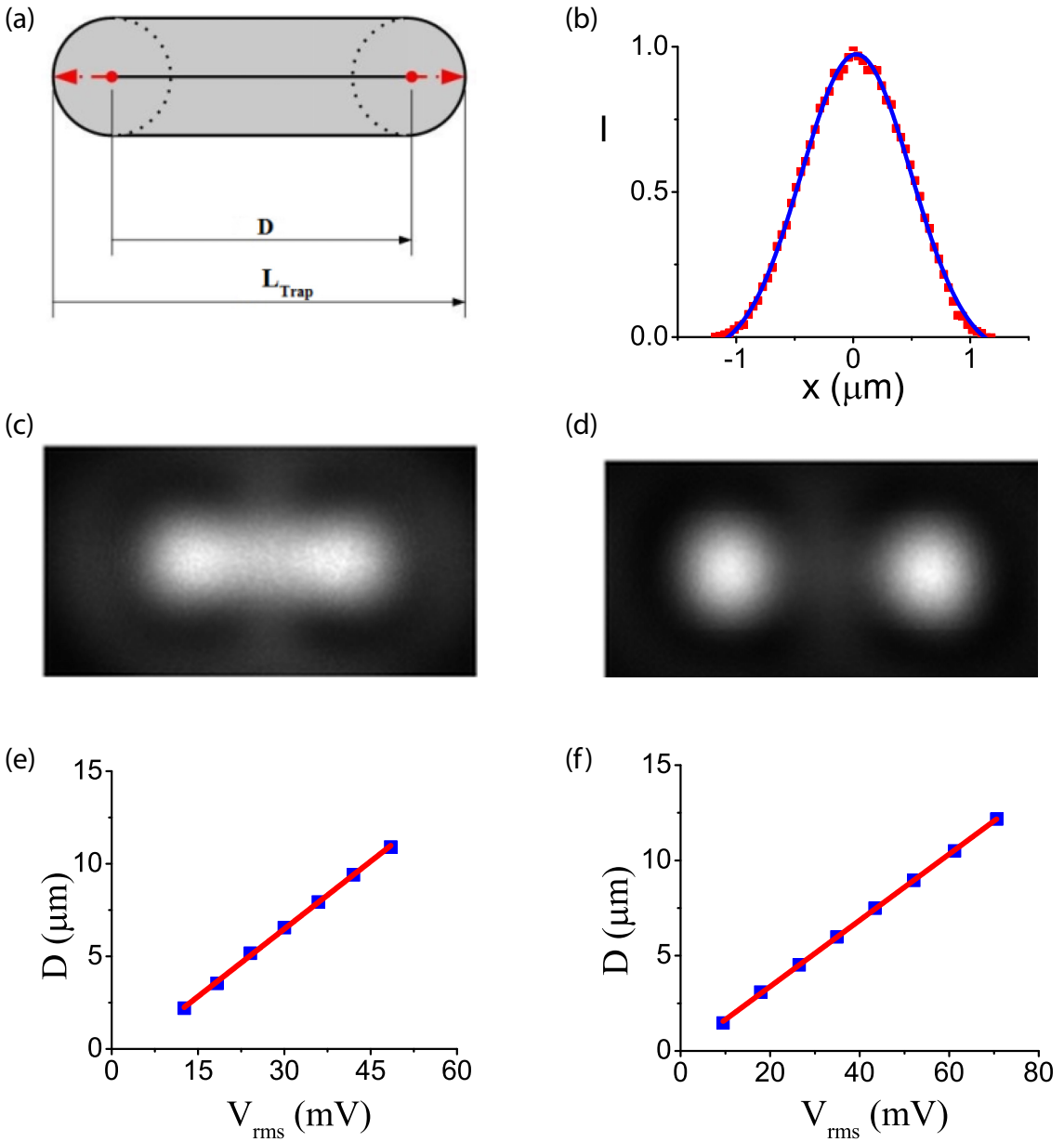

FIG. 1. Behavior of the oscillating tweezers. (a) Schematic diagram of the sinusoidally oscillating laser beam. It describes the time-averaged intensity distribution in the focal plane, $I(x,y)$, where D is the distance between the $I(x,y)$ maxima and L_{trap} is the trap length. Moreover, $L_{\text{trap}} = D + d$, where d is the full width at half maximum (FWHM) of the nonoscillating laser beam intensity profile in the focal plane. (b) Normalized intensity profile, $I(x)$, of the nonoscillating laser beam in the focal plane (red squares) together with the Gaussian that represents the best fit to $I(x)$ (red line, FWHM $= 1.10 \pm 0.01\,\mu$m). (c) Images of the oscillating laser beam $I(x,y)$ for sinusoidal voltage at 100 Hz and $V_{\text{rms}} = 12.6$ mV. (d) Same as in panel (c) for a square wave voltage and $V_{\text{rms}} = 17.9$ mV. (e) The distance between the two maxima of $I(x,y)$, D, as a function of the oscillating voltage, V_{rms}, at 100 Hz frequency for the sinusoidal voltage (blue squares). The red line represents the best linear fit to the data. (f) Same as in panel (e) for the square wave voltage.

that, in the range of small oscillation amplitudes, where the two peaks of $I(x,y)$ significantly overlap, the dependence of D on V_{rms} will deviate from its linear behavior, vanishing at a finite value of the voltage.

C. Sample preparation

To test the trapping stability in oscillating tweezers we used fixed *E. coli* cells (EC448 [24]). Cells were grown in Luria-Bertani liquid medium (LB) till 0.2 optical density, $\text{OD}_{600} =$ 0.2, in the exponential growth regime. Next, cells were fixed using 0.2% formaldehyde. For microscopy, 30 μl of fixed cells were placed in the sample chamber (see Sec. II A).

D. Measuring center of mass and orientation angles of trapped *E. coli*

To measure the fluctuations of cells trapped in oscillating tweezers, these were monitored using phase contrast imaging in an appropriate range of trap lengths and trapping beam

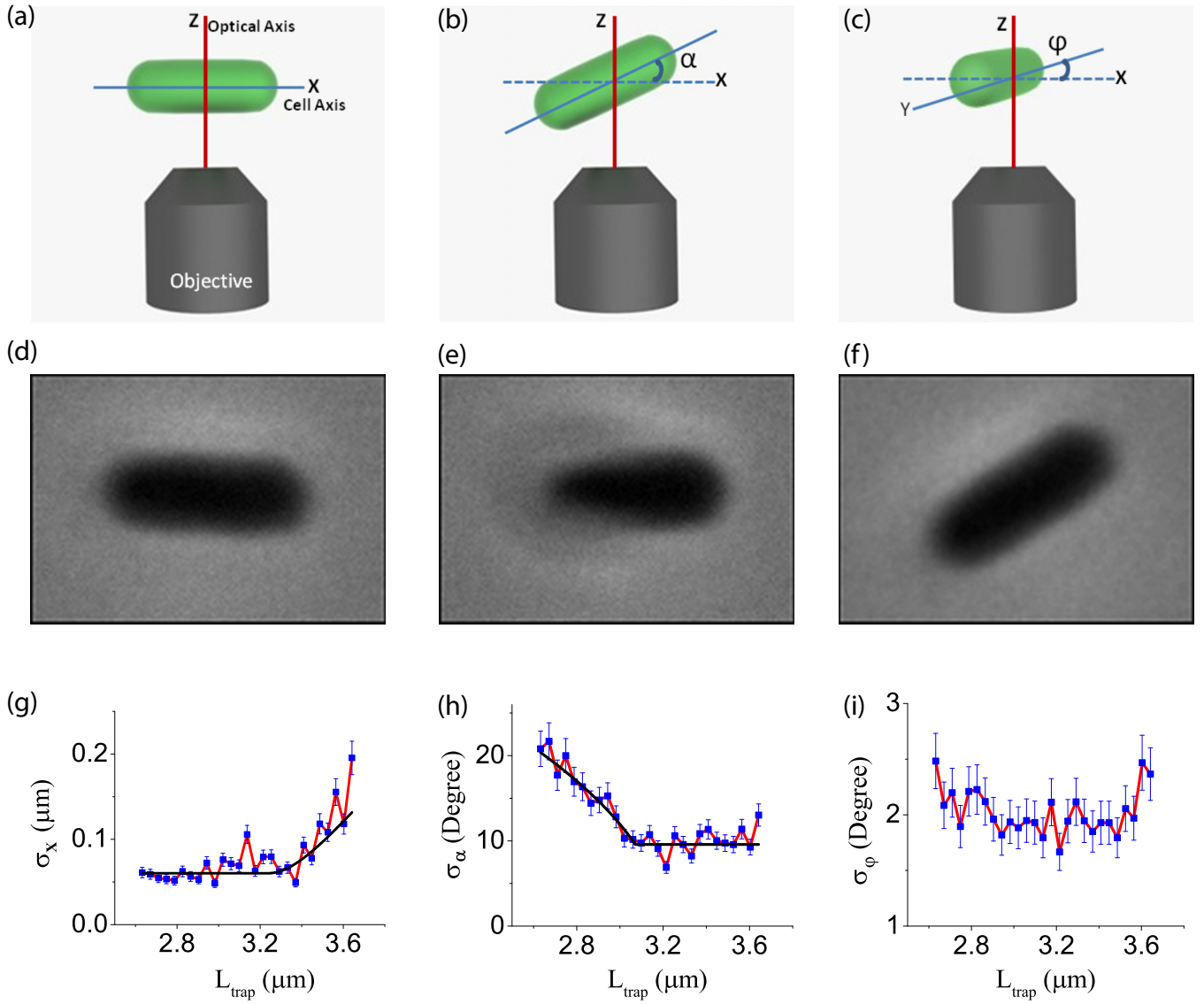

FIG. 2. Fluctuations of the trapped cell. (a) Schematic diagram of the horizontally aligned cell in the trap. Illustration of the cell rotation angles, (b) relative to the focal plane, α, and (c) within the focal plane, φ. (d) Image of a horizontally aligned trapped cell. (e) Same cell as in panel (d) rotated at an angle out of the focal plane, $a = 17^{\circ}$. The image corresponds to a relatively large angle shown to emphasize the effect of such rotation. (f) Illustration of the effect on the cell image of rotation within the focal plane. Since in our system the fluctuations in φ are rather small, here we show the same image as in (d) only rotated by 30°. (g) Dependence of the standard deviation (σ) of $x_{\rm cm}$, σ_x, as a function of the trap length, $L_{\rm trap}$ (blue squares). Error bars correspond to the error of the standard deviation (see text) and $L_{\rm cell} = 3\,\mu$m (cell II). To guide the eye, a line connects between the data points (red line). For comparison, the best fit of Eq. (1) to the $\sigma_x(L_{\rm trap})$ data is also shown (black line). (h) Same as in panel (g) only for the standard deviation of the angle α, σ_α. Here we use Eq. (2) to fit the $\sigma_\alpha(L_{\rm trap})$ data (black line). (i) Same as in panel (g) only for the standard deviation of the angle φ, σ_φ.

powers. For each cell and set of trap parameters, we recorded 50 frames with 20 ms exposure time and about 200 ms between consecutive frames. Using MATLAB (MathWorks), cell images were analyzed to obtain the contours best approximating the position of the cytoplasmic membrane (CM) in the focal plane. To this end, we used an approach that was previously developed in our lab [25,26]. It involves a calibration stage whereby we measure the phase contrast intensity corresponding to the CM. Fixed cells are labeled with FM4-64 staining the CM and each one is imaged in both fluorescence and phase contrast modes. Assuming that the position of the cell is the same in the two images and that the pixels along the high intensity ridge in the fluorescence image locate the CM, this allows tracing the CM in the corresponding phase contrast image. Averaging the phase contrast intensity along the CM and for N_c different cells, $N_c = 7$, we obtain an intensity threshold value that approximates the position of the CM in phase contrast images. The CM contours are obtained with subpixel accuracy using two-dimensional linear interpolation.

Trapping stability in the oscillating tweezers was characterized in terms of four of the cell coordinates, namely, its (x,y) center of mass coordinates, $x_{\rm cm}$ and $y_{\rm cm}$, the angle with respect to the (x,y) plane, α, and the azimuthal angle [in the (x,y) plane], φ [see Figs. 2(a)–2(f)]. For each cell image, the

values of these coordinates were estimated using the cell CM contours. For example, x_{cm} and y_{cm} were obtained by averaging the x and y coordinates, respectively, of the cell contour points. Another two coordinates, namely, the fluctuations of the center of mass in the z direction, z_{cm}, and the rotation angle around the long cell axis, χ, cannot be obtained from the cell contours requiring a different approach. We postpone the stability analysis of the z_{cm} and χ coordinates for future studies (see Conclusions).

To approximate the angle between the cell axis and the focal plane, α, we define the length of the cell contour as the maximal distance between any two contour points. For images where both caps of the trapped cell appear to be equally focused, $\alpha \approx 0$, the length of the cell contour corresponds to the cell length, L_{cell}. In contrast, the contours of cells that are inclined with respect to the (x,y) plane, $\alpha \neq 0$, approximate the projection of the cell edge on the focal plane. In this case, the length of the cell contour is shorter than L_{cell} by a factor of $\cos(\alpha)$ allowing us to determine the absolute value of α, $|\alpha|$, but not its sign. We note that for large α the contour detection algorithm becomes inaccurate due to the cell caps becoming too defocused. Consequently, our approach is limited to the range of small angles. Nevertheless, a slight generalization of this method was shown to extend its validity up to $\alpha \approx 70^\circ$ [14].

To obtain the azimuthal angle, φ, we first removed from the cell contour the two, approximately semicircular, cap sections. Next, we used the best linear fit to each of the remaining lateral sections of the cell contour and averaged the corresponding two slopes to estimate the value of φ.

For cells trapped in oscillating tweezers, the four cell coordinates that we measure, x_{cm}, y_{cm}, α, and φ, fluctuate around equilibrium values. The average center of mass, $(\langle x_{cm}\rangle, \langle y_{cm}\rangle)$, coincides with the center of the trap and the average angles vanish, $\langle\alpha\rangle = 0$ and $\langle\varphi\rangle = 0$. Therefore, to quantify the stability of the trapping we use the standard deviations (σ) of the measured coordinates [Figs. 2(g)–2(i) and 3]. For each cell and set of trap parameters, the σ's are computed from the corresponding 50 frame time lapse movie. Although in the case of the angle α, our approach only allows to measure $\langle|\alpha|\rangle$, assuming a Gaussian distribution for α, it can be shown that $\sigma_\alpha = \sqrt{\pi/2}\langle|\alpha|\rangle$ [27]. Moreover, assuming that all four coordinates are Gaussian distributed allows us to obtain the error of their standard deviations, $\Delta\sigma = \sigma/\sqrt{2N}$ [27]. Here, N denotes the number of frames.

III. RESULTS

Rod-shaped cells can be trapped and horizontally aligned in oscillating tweezers. The main parameters that affect the stability of the trapped cells are the trap length and the trapping power.

A. Cell trapping stability in oscillating tweezers–Dependence on trap length

To analyze the effect of the trap length on the stability of the trapped cell we first used a simple approach whereby the extent of the fluctuations is compared by visual inspection. For each cell, we scan the trap length, L_{trap}, and

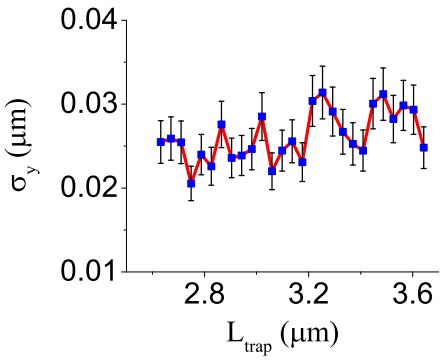

FIG. 3. Fluctuations of the trapped cell. Same as in Fig. 2(g) only for the standard deviation of y_{cm}, σ_y.

appreciate for which value is the cell most stably trapped. Repeating the experiment for cells of varying length, L_{cell}, we find that trapping stability is best for values of L_{trap} that, to a good approximation, depend linearly on the cell length, $L_{trap} = a\,L_{cell} + b$, where $a = 0.5 \pm 0.1$ and $b = 1.3 \pm 0.3\,\mu$m (Fig. 4). Assuming the smallest cells to be 2.5 μm long, this relation suggests that for short cells the length of the most stable trap is approximately equal to the cell length, e.g., $L_{trap}(2.5\,\mu\text{m}) = 2.5 \pm 0.4\,\mu$m. In contrast, for longer cells the optimal trap length becomes gradually smaller than the cell length itself, e.g., $L_{trap}(4\,\mu\text{m}) = 3.3 \pm 0.5\,\mu$m. This result seems to contradict our previous observations that whenever the length of the trap becomes smaller than the cell length, the cell will align at a certain angle with the focal plane, $\alpha \neq 0$ [13,14]. However, in the past we only studied cells that were about 3 μm long. Moreover, the fluctuations in the optimal trap length data of Fig. 4 and the corresponding errors in the fit parameters are relatively large, suggesting that we should further analyze this behavior before drawing conclusions.

For a more accurate analysis of the trapping stability, we have studied the fluctuations of each of the four cell coordinates that we measure from the CM contours, x_{cm}, y_{cm}, α, and φ, (see Sec. II), as a function of the trap length [Figs. 2(g)–2(i) and 3].

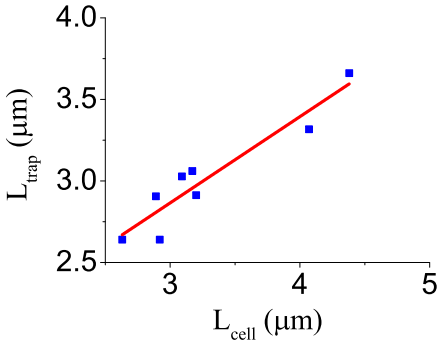

FIG. 4. Dependence of the optimal trap length on the length of the cell. For different cells we determine the trap length where the trapping is most stable by visual inspection. The data for $L_{trap}(L_{cell})$ (blue squares) is compared to the corresponding best linear fit (red line), $L_{trap} = a\,L_{cell} + b$, where $a = 0.5 \pm 0.1$ and $b = 1.3 \pm 0.3\,\mu$m. Here we use L_{trap} to denote the particular trap length where the cell is most stably trapped.

The fluctuations of the trapped cell center of mass position along the x axis, x_{cm}, are nearly constant as long as the trap length is smaller than the cell length, $L_{trap} < L_{cell}$, and increase gradually after exceeding the cell length, $L_{cell} = 3\,\mu$m [cell II, Figs. 2(g)]. Regarding the oscillating tweezers as a linear trap [see Fig. 1(c)] provides a simple framework to understand this behavior. In the range where $L_{trap} < L_{cell}$, cell motion along the x axis is limited to within the boundaries of the trap. Accordingly, the fluctuations of x_{cm} are of similar nature to those of a microbead in a relatively weak steady optical trap. This description only holds as long as L_{trap} is moderately shorter than the cell length. At shorter trap lengths, the cell will significantly deviate from the horizontal orientation (large α), leading to weaker trapping in the x direction and correspondingly, to larger fluctuation in x_{cm}. This regime is not directly relevant to the stability of horizontal trapping and therefore is beyond the scope of this study. In contrast, when the trap length is larger than the cell length, the cell can fluctuate freely in the x direction before it encounters the walls of the trapping potential. In this case, one may assume that the fluctuations in x_{cm} are the sum of the same thermal component as in the $L_{trap} < L_{cell}$ range and a fluctuation uniformly distributed in the L_{trap}–L_{cell} range. This description leads to a simple dependence of the standard deviation, $\sigma_{x,t}$, on the trap length, L_{trap},

$$\sigma_{x,t}(L_{trap}) = \begin{cases} a & L_{trap} < L_{cell} \\ \sqrt{a^2 + \left(\frac{L_{trap} - L_{cell}}{2\sqrt{3}}\right)^2} & L_{trap} > L_{cell} \end{cases}, \quad (1)$$

which, in turn, is in good agreement with the data of Fig. 2(g) when we use both a and L_{cell} as fitting parameters. The best fit is obtained for a $= 60 \pm 3$ nm and $L_{cell} = 3.24 \pm 0.03\,\mu$m. The fact that the cell length obtained from the fit is larger than the true cell length (3 μm) reflects the limited accuracy of the uniform distribution assumption for the fluctuations in the L_{trap}–L_{cell} range. Since the average trapping beam intensity is larger at the edges of the trap than at its center [Fig. 1(c)], cells are also expected to prefer positions closer to the trap edges.

Within the accuracy of our experiment, the dynamics of the cell center of mass in the y direction, y_{cm}, is apparently independent of the trap length (Fig. 3). This is precisely the expected behavior in the case of a linear trap where the trapping potential in the y direction is homogeneous all along the trap. It shows that sinusoidally oscillating tweezers are well approximated as a linear trap.

While the fluctuation behavior of the center of mass coordinates is relatively straightforward, that of the angle of the cell with respect to the focal plane, α, is slightly more complex [Fig. 2(h)]. Specifically, α, displays a sudden increase in its fluctuations when L_{trap} becomes smaller than the cell length [Fig. 2(h). In the range where $L_{trap} > L_{cell}$, the linear trap tends to confine the cell to the focal plane and fluctuations in α are due to rotational Brownian motion around the $\alpha = 0$ equilibrium. In contrast, when $L_{trap} < L_{cell}$, the caps of a horizontally aligned cell exceed the range of the trapping potential and experience no significant restoring force. It is therefore preferable for the cell to align at a finite α such that the trapping potential will act on its entire volume. Since the trapping force decreases as we move away from the focal plane, the most stable trapping is achieved at about the smallest α where the cell is fully within the trap, $\cos|\alpha| \approx L_{trap}/L_{cell}$. However, the cell is equally stable in both the α and -α orientations. For small values of $|\alpha|$, the cell will readily hop between the α and -α orientations leading to fluctuations in α that grow as the length of the trap decreases. Using a similar argument as the one leading to Eq. (1), we describe the fluctuations in α as being the result of two contributions, one due to thermal fluctuations and the second in the form of a uniformly distributed angle in the (-α, α) range. The corresponding standard deviation,

$$\sigma_{\alpha,t}(L_{trap}) = \begin{cases} \sqrt{c^2 + \frac{1}{3}\left(a\cos\left(\frac{L_{trap}}{L_{cell}}\right)\right)^2} & L_{trap} < L_{cell} \\ c & L_{trap} > L_{cell} \end{cases}, \quad (2)$$

is expected to provide a good description of the σ_α (L_{trap}) data. Indeed, the best fit of $\sigma_{\alpha,t}$ (L_{trap}) to the data with c and L_{cell} as parameters corresponds to $c = 9.6 \pm 0.3^\circ$ and $L_{cell} = 3.07 \pm 0.02\,\mu$m and provides a good approximation to the data. Although like in the case of the fluctuations along the x direction, the L_{cell} value obtained from the fit is larger than the true cell length (3 μm), here the two values are much closer. This suggests that the uniform α-angle distribution assumption leading to Eq. (2) is relatively accurate.

Understanding the fluctuation behavior of the angle φ [Fig. 2(i)] requires that we move beyond the linear trap approximation and consider the fact that for the sinusoidally oscillating tweezers the trapping force is stronger at the end sections of the trap than at its center [Fig. 1(c)]. Therefore, in the $L_{trap} > L_{cell}$ regime, the cell cannot simultaneously benefit from both regions of strong trapping at the ends of the trap which, in turn, leads to larger fluctuations in φ than for $L_{trap} \approx L_{cell}$ [Fig. 2(i)]. Similarly, when $L_{trap} < L_{cell}$, at least one of the cell ends lies off the focal plane experiencing a weaker trapping potential than in the focal plane. Such inclined orientation, $|\alpha| > 0$, leads to an increased value of σ_φ relative to the range where $\alpha \approx 0$ [Fig. 2(i)].

To test the dependence of the trapping stability on the cell length we analyzed the behavior of σ_x (L_{trap}), σ_y (L_{trap}), σ_α (L_{trap}), and σ_φ (L_{trap}) for cells of different length, $L_{cell} = 2.52\,\mu$m (cell I), 3.15 μm (cell III), 3.28 μm (cell IV), 3.45 μm (cell V), 3.57 μm (cell VI), 3.99 μm (cell VII), and 4.53 μm (cell VIII) (Figs. S3–S9). While the overall behavior of the fluctuations in these 7 cells is similar to that in cell II, one also finds some deviations from the expected dependence on L_{trap}. The main discrepancy is that the behavior of σ_φ (L_{trap}) observed in Fig. 2(i) showing a minimum in the $L_{trap} \approx L_{cell}$ range, does not manifest in any of the other cells being probably smaller than the experimental noise [Figs. S3(d)–S9(d)]. It is therefore a good approximation to assume that σ_φ is practically independent of L_{trap}. Further unexpected behavior is found for cell V where σ_α (L_{trap}) at $L_{trap} > L_{cell}$ grows toward large values instead of remaining at about the same value as in the $L_{trap} \approx L_{cell}$ range [Fig. S5(b)]. However, considering that our data is obtained from measurements on individual cells, it is natural to expect some variability in the trapping stability.

Since each of the four cell coordinates that we analyzed, x_{cm}, y_{cm}, α, and φ, behaves differently as a function of L_{trap}, it

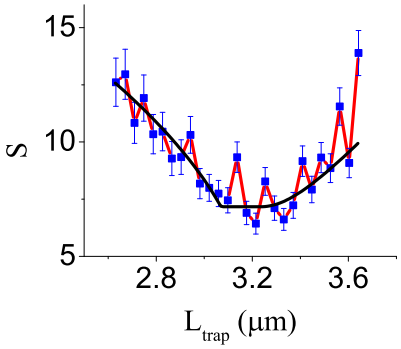

FIG. 5. Dependence of the stability variable, S, on L_{trap} for the same cell as in Figs. 2(g)–2(i) and 3 (cell II, $L_{\text{cell}} = 3\,\mu$m, blue squares). Error bars represent the error of S, ΔS, obtained from the errors of σ_x, σ_θ, $\langle\sigma_y\rangle$, $\langle\sigma_\varphi\rangle$ and Eq. (3). To guide the eye, a line connects between the data points (red line). For comparison, the theoretical behavior of $S(L_{\text{trap}})$ corresponding to the prediction of Eqs. (1) and (2) with the corresponding parameters obtained from the best fit of each of the four coordinates, x_{cm}, y_{cm}, α, and φ, is also shown (black line).

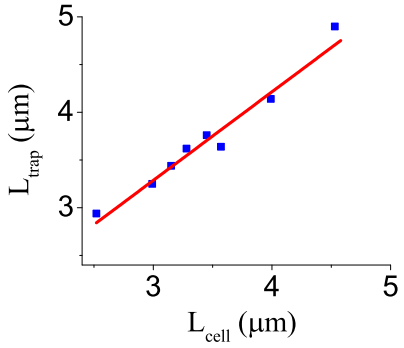

FIG. 6. Dependence of the optimal trap length on the length of the cell. For different cells we determine the trap length where the trapping is most stable. It corresponds to the minimum of the stability variable, S, as a function of L_{trap}. The data for $L_{\text{trap}}(L_{\text{cell}})$ (blue squares) is compared to the corresponding best linear fit (red line), $L_{\text{trap}} = a\,L_{\text{cell}} + b$, where $a = 0.95 \pm 0.07$ and $b = 0.4 \pm 0.3\,\mu$m. Here we use L_{trap} to denote the particular trap length where the cell is most stably trapped.

is not straightforward to determine the trap length where the cell is most stably trapped with respect to these coordinates. In particular, while σ_x grows with L_{trap} [Fig. 2(g)], σ_α displays an opposite trend [Fig. 2(h)]. This requires finding an optimal compromise between the behaviors of the different cell coordinates where the cell fluctuations are minimal. To this end, we define a composite coordinate, S,

$$S = \frac{\boldsymbol{\sigma}_x}{\langle\boldsymbol{\sigma}_y\rangle} + \frac{\boldsymbol{\sigma}_\alpha}{\langle\boldsymbol{\sigma}_\varphi\rangle}, \tag{3}$$

where $\langle\sigma_y\rangle$ and $\langle\sigma_\varphi\rangle$ are the standard deviations of the y_{cm} and φ coordinates, respectively, averaged over the entire range of L_{trap} that was scanned for a particular cell. In defining the S variable, we have assumed that the trapping stability is mainly determined by the variation of σ_x and σ_α, while both σ_y and σ_φ are either constant or do not significantly vary over the relevant range of L_{trap} values. Accordingly, we use the average values of σ_y and σ_φ to normalize the behavior of σ_x and σ_α, respectively. In Fig. 5 we show the behavior of S as a function of the trap length for the same cell as in Figs. 2(g)–2(h) and 3 (cell II) and compare it to the prediction of Eqs. (1) and (2) with the corresponding parameters obtained from the best fit of each of the four coordinates, x_{cm}, y_{cm}, α, and φ. As expected, the experimental $S(L_{\text{trap}})$ has a clear minimum in the vicinity of $L_{\text{trap}} \approx L_{\text{cell}}$. Assuming that the S-variable represents the proper measure of trapping stability, the value of L_{trap} corresponding to the minimum of $S(L_{\text{trap}})$ corresponds to the most stable configuration of the oscillating tweezers. We note that for the $S(L_{\text{trap}})$ obtained from Eqs. (1) and (2), S is minimal within a relatively small interval of trap lengths that contains the minimum of the experimental $S(L_{\text{trap}})$.

Since the dependence of the S variable on L_{trap} is not particularly smooth, we use polynomial interpolation to determine the position of its minimum. To this end, we fit the data with a third order polynomial to account for the asymmetry of $S(L_{\text{trap}})$. The values of L_{trap} corresponding to the interpolated minimum of $S(L_{\text{trap}})$ were obtained for all the eight cells that were analyzed [Figs. 5 and S3(e)–S9(e)] leading to a quantitative version of Fig. 4 (see Fig. 6). Here, the linear approximation for the behavior of the optimal L_{trap} with L_{cell} is significantly more accurate than in Fig. 4 and the best linear fit to the $L_{\text{trap}}(L_{\text{cell}})$ data is, $L_{\text{trap}} = a\,L_{\text{cell}} + b$, where $a = 0.95 \pm 0.07$ and $b = 0.4 \pm 0.3\,\mu$m.

On the qualitative level, the behavior found in Fig. 6 is similar to that of Fig. 4. However, here we find that the best linear fit to the $L_{\text{trap}}(L_{\text{cell}})$ data has an approximately unit slope and the value of $L_{\text{trap}}(0)$ is sufficiently small to be consistent with a vanishing $L_{\text{trap}}(0)$ considering that the shortest cell we measured was 2.52 μm long. One may therefore conclude that, within the accuracy of our experimental approach, the optimal trap length is equal to the cell length, $L_{\text{trap}} \approx L_{\text{cell}}$.

B. Cell trapping stability in oscillating tweezers–Dependence on the trapping beam power

Another important factor that determines the trapping efficiency of our setup is the power of the trapping beam, P. To understand the dependence of the trapped cell fluctuations on P in oscillating tweezers, we first analyzed the fluctuations of trapped polystyrene beads in the nonoscillating trap [27]. Using Stokes force calibration, we obtain that the parameter characterizing the OT trapping efficiency, β [see Eq. (S2)], is $0.17 \pm 0.02\,\mu\text{m}^{-1}$ for microbeads of 0.8 μm radius. Moreover, we show that the thermal fluctuations of the microbeads, e.g., σ_x^2, are inversely proportional to P [27].

Next, analyzing the thermal fluctuations of trapped cells in oscillating tweezers in each of the four coordinates that we measure using cell contours, we find that these are also inversely proportional to P. Although a 3 μm long *E. coli* cell has about the same volume as a 0.8 μm radius polystyrene bead and using the trap length that minimizes the S coordinate [Eq. (3)], the trapping of the cells is significantly weaker. First, this is due to the much smaller difference in refraction index between the cell (1.388) and the medium (water, 1.323) relative to the case of polystyrene, $n = 1.578$. Second, in oscillating tweezers, on average, the beam power is spread over the entire extent of the trap length, L_{trap}. For example, the

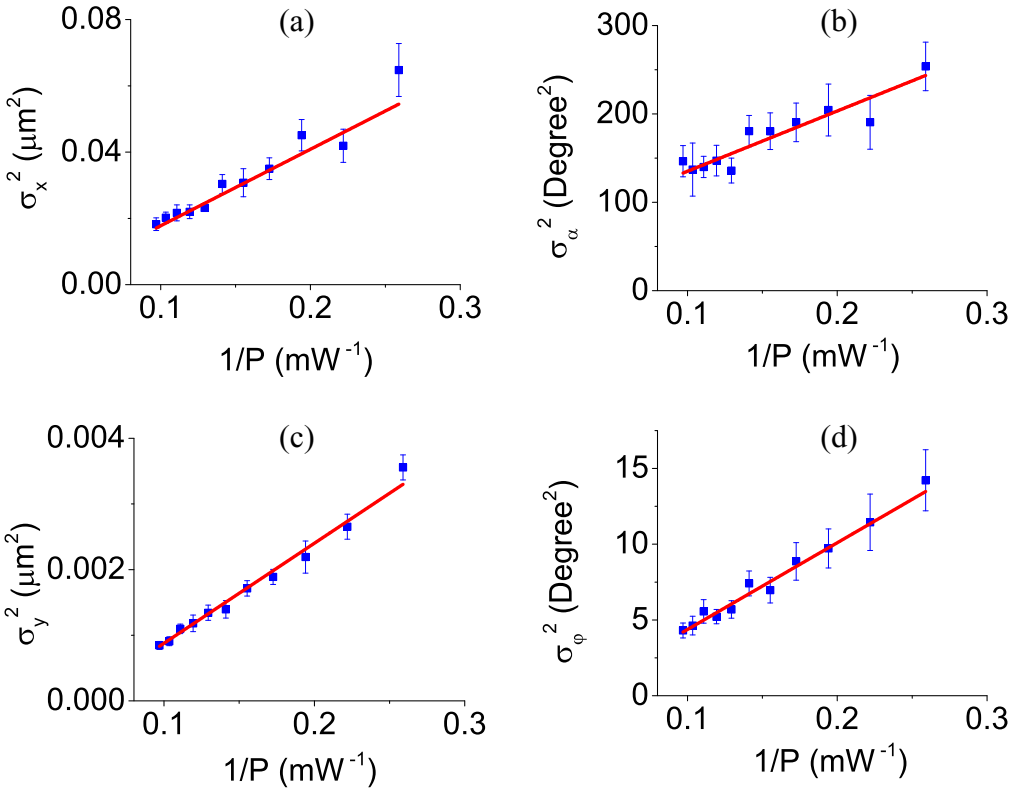

FIG. 7. Dependence of cell trapping stability on the inverse of the trapping beam power, P^{-1}. The data represents averages over 10 cells that are all around 3 μm long ($\langle L_{\rm cell}\rangle = 3.1\,\mu$m, $\sigma_{L\rm cell} = 0.3\,\mu$m). For each of the 10 cells, $L_{\rm trap}$ is set to the value that minimizes the $S(L_{\rm trap})$ function according to the prediction of the best fit in Fig. 6. Error bars correspond to the standard error of the 10-cell average. (a) The variance of $x_{\rm cm}$, $(\sigma_x)^2$, as a function of P^{-1} (blue squares) is shown together with the corresponding best linear fit (red line). (b) Same as in panel (a) only for the variance of the angle α, $(\sigma_\alpha)^2$. (c) Same as in panel (a) only for the variance of $y_{\rm cm}$, $(\sigma_y)^2$. (d) Same as in panel (a) only for the variance of the angle φ, $(\sigma_\varphi)^2$.

maximal intensity in the beam image in Fig. 1(c) is 2.35 times lower than the corresponding value for the nonoscillating beam. Nevertheless, the thermal fluctuations of the center of mass coordinates for a trapped cell in the oscillating tweezers are also inversely proportional to the total trapping power, P [Figs. 1(a) and 1(c)]. This allows us using Eq. (S4) to define effective values of β for each of the $x_{\rm cm}$ and $y_{\rm cm}$ coordinates, β_x and β_y, respectively. Specifically, fitting the average $\sigma_x^2(P^{-1})$ and $\sigma_y^2(P^{-1})$ taken over 10 cells of about the same length (∼3 μm) we obtain $\beta_x = 0.0041 \pm 0.0004\,\mu{\rm m}^{-1}$ and $\beta_y = 0.062 \pm 0.002\,\mu{\rm m}^{-1}$, respectively [Figs. 7(a) and 7(c)]. As expected, both β_x and β_y are much smaller than the value for the polystyrene bead and, moreover, $\beta_x \ll \beta_y$. The fact that β_x is smaller that β_y is due to both the softer walls along the x axis and the larger freedom of rotation in α relative to that in φ. The softer x wall manifests in the beam intensity distribution of Fig. 1(c), where the intensity at the extremes of the trap decays at a slower rate along the x axis than along the y axis. Moreover, a large deviation in α leads to a projected cell length along x that is smaller than the trap length allowing the cell additional freedom to fluctuate in x within the boundaries of the trap.

The discussion that leads to the power dependence of the coordinate thermal fluctuation, σ_x^2 (P) [see Eq. (S4)] [27] can be readily generalized to describe the corresponding behavior of rotational fluctuations of a rodlike object. The analogy relies on the fact that, similar to the case of the bead-trapping effective potential, for small rotations around the equilibrium position, the angles will experience a linear restoring torque. Accordingly, one expects that both σ_α^2 and σ_φ^2 are proportional to the inverse trapping power, P^{-1}, and may define β_α and β_φ, respectively. From the corresponding linear fits to the averaged $\sigma_\alpha^2(P^{-1})$ and $\sigma_\varphi^2(P^{-1})$ over 10 different cells of about the same length [Figs. 7(b) and 7(d)] we obtain $\beta_\alpha = (0.46 \pm 0.07)10^{-6}\,{\rm deg}^{-2}$ and $\beta_\varphi = (5.5 \pm 0.4)10^{-6}\,{\rm deg}^{-2}$. The fluctuations in α are significantly larger than those in φ due to the much smaller trapping beam intensity gradient along the z axis relative to that along the y axis.

IV. CONCLUSIONS

We have shown that rod-shaped cells trapped in oscillating tweezers fluctuate differently in each of the four cell coordinates that we analyzed, $x_{\rm cm}$, $y_{\rm cm}$, α, and φ, both for a particular set of trap parameters and as a function of the trap length, $L_{\rm trap}$. While the fluctuations of the center of mass x coordinate, $x_{\rm cm}$, grow as $L_{\rm trap}$ increases [Figs. 2(g) and S3(a)–S9(a)], those in the angle between the cell and the focal plane, α, decrease as $L_{\rm trap}$ grows [Figs. 2(h) and S3(b)–S9(b)]. In contrast, the fluctuations in both $y_{\rm cm}$ and φ are only weakly dependent on $L_{\rm trap}$ and may be regarded as practically constant [Figs. 2(i), S3(c)–S9(c), 3, and S3(d)–S9(d)]. Moreover, the variances

of these cell coordinates are apparently proportional to the inverse of the trapping beam power (Fig. 7) and, as expected, are independent of the oscillation frequency in the range between 40 and 200 Hz (Fig. S2).

Optimizing the trapping of rod-shaped cells, we obtain that the trap length should be about the same as the cell length to minimize fluctuations in the four coordinates that we analyzed. Specifically, we find that whenever $L_{\mathrm{trap}} = a\,L_{\mathrm{cell}} + b$, where $a = 0.95 \pm 0.07$ and $b = 0.4 \pm 0.3\ \mu$m, a variable that sums up the fluctuations in x_{cm} and α is minimized (Fig. 6). One may conclude that, to a good approximation, cell trapping in oscillating OT is most stable when $L_{\mathrm{trap}} = L_{\mathrm{cell}}$.

We note that, in the optimized range, the fluctuations of x_{cm} and α are significantly larger than those of y_{cm} and φ [Figs. 2(g)–2(i), 3, and S3-S9], respectively. The standard deviation of x_{cm} in this range, σ_x, is ∼80 nm, while $\sigma_y \approx 30$ nm for cell II [Figs. 2(g) and 3, $L_{\mathrm{cell}} = 3\ \mu$m]. Similarly, for cell II, $\sigma_\alpha \approx 10^\circ$, while $\sigma_\varphi \approx 2^\circ$ [Figs. 2(h) and 2(i)]. Since along the x axis the trap boundaries are not as steep as those in the y direction, the x_{cm} fluctuations are larger than those of y_{cm}. Like in the nonoscillating trap, the trapping potential is weaker in the z direction than in the y direction. This results in larger fluctuations in the angle with respect to the focal plane, α, relative to those in the azimuthal angle, φ.

As discussed in Sec. II D, the trapping stability of the center of mass in the z direction, z_{cm}, and of the rotational angle around the long cell axis, χ, cannot be obtained from the analysis of the cell contours as in the case of the four cell coordinates that were discussed in our study. To measure z_{cm}, one may analyze the extent of cell image defocusing, e.g., using the intensity gradient along the cell contour. Moreover, one may attach small fluorescent microbeads (e.g., 0.1 μm diameter) to the cell outer membrane to monitor the dynamics of the χ angle. While we postpone these studies to future work, results from imaging trapped *E. coli* cells in double beam OT suggest that the fluctuations in χ may be negligible. Diekmann *et al.* [12] imaged the nucleoids of trapped cells at four consecutive time intervals of about 22 s and found practically the same fluorescence intensity distribution in all of them. They proposed that the variation of the refraction index within the cell is sufficient to break the apparent rotational symmetry in χ as to trap the cell in a particular χ orientation.

For rod-shaped cells, trapping stability is not determined by the fluctuations of the cell center of mass alone. Instead, it is also affected by the rotational fluctuations of the trapped cell. We have shown that the angular fluctuations in α and φ are no less important for the cell trapping stability than those of the center of mass. In particular, trapping is most stable when a balance between the opposite trends of angular and center of mass fluctuations is attained. Notably, a careful generalization of the deconvolution approach to the imaging of trapped cells introduced in Ref. [12] to include angular fluctuations may lead to significantly improved imaging accuracy. To allow monitoring live cells over long time intervals it is necessary to reduce the extent of photodamage due to the trapping laser beam. This can be achieved using free radical scavengers, e.g., ascorbic acid, which were found to preserve the growth rate of *E. coli* for times at least as long as 60 min [28].

Note added in proof. Another paper was recently published presenting a related study on trapping rod-shaped bacteria using oscillating optical tweezers [29].

ACKNOWLEDGMENT

We thank I. Fishov and R. Granek for useful discussions. This research was supported in part by the Israel Academy of Science and Humanities (Grants No. 1701/13 and No. 1519/18).

[1] S. M. Block, D. F. Blair, and H. C. Berg, Compliance of bacterial flagella measured with optical tweezers, Nature **338**, 514 (1989).

[2] K. Svoboda, C. F. Schmidt, D. Branton, and S. M. Block, Conformation and elasticity of the isolated red blood cell membrane skeleton, Biophys. J. **63**, 784 (1992).

[3] M. Sato-Maeda, M. Uchida, F. Graner, and H. Tashiro, Quantitative evaluation of tissue-specific cell adhesion at the level of a single cell pair, Dev. Biol. **162**, 77 (1994).

[4] A. Ashkin, J. M. Dziedzic, and T. Yamane, Optical trapping and manipulation of single cells using infrared laser beams, Nature **330**, 769 (1987).

[5] T. N. Buican, M. J. Smyth, H. A. Crissman, G. C. Salzman, C. C. Stewart, and J. C. Martin, Automated single-cell manipulation and sorting by light trapping, Appl. Opt. **26**, 5311 (1987).

[6] S. Seeger, S. Monajembashi, K. J. Hutter, G. Futterman, J. Wolfrum, and K. O. Greulich, Application of laser optical tweezers in immunology and molecular genetics, Cytometry **12**, 497 (1991).

[7] R. W. Steubing, S. Cheng, W. H. Wright, Y. Numajiri, and M. W. Berns, Laser induced cell fusion in combination with optical tweezers: the laser cell fusion trap, Cytometry **12**, 505 (1991).

[8] J. A. Grimbergen, K. Visscher, D. S. Gomes de Mesquita, and G. J. Brakenhoff, Isolation of single yeast cells by optical trapping, Yeast **9**, 723 (1993).

[9] M. Goksor, J. Enger, and D. Hanstorp, Optical manipulation in combination with multiphoton microscopy for single-cell studies, Appl. Opt. **43**, 4831 (2004).

[10] C. Creely, G. Volpe, G. Singh, M. Soler, and D. Petrov, Raman imaging of floating cells, Opt. Express **13**, 6105 (2005).

[11] M. Werner, F. Merenda, J. Piguet, R. P. Salathe, and H. Vogel, Microfluidic array cytometer based on refractive optical tweezers for parallel trapping, imaging and sorting of individual cells, Lab Chip **11**, 2432 (2011).

[12] R. Diekmann, D. L. Wolfson, C. Spahn, M. Heilemann, M. Schuttpelz, and T. Huser, Nanoscopy of bacterial cells immobilized by holographic optical tweezers, Nat. Commun. **7**, 13711 (2016).

[13] G. Carmon and M. Feingold, Rotation of single bacterial cells relative to the optical axis using optical tweezers, Opt. Lett. **36**, 40 (2011).

[14] G. Carmon and M. Feingold, Controlled alignment of bacterial cells with oscillating optical tweezers, J. Nanophoton. **5**, 051803 (2011).

[15] R. M. Berry and H. C. Berg, Absence of a barrier to backwards rotation of the bacterial flagellar motor demonstrated with optical tweezers, Proc. Natl. Acad. Sci. USA **94**, 14433 (1997).

[16] J. Jass, S. Schedin, E. Fallman, J. Ohlsson, U. J. Nilsson, B. E. Uhlin, and O. Axner, Physical properties of *Escherichia coli* P pili measured by optical tweezers, Biophys. J. **87**, 4271 (2004).

[17] K. Visscher, G. J. Brakenhoff, and J. J. Krol, Micromanipulation by "multiple" optical traps created by a single fast scanning trap integrated with the bilateral confocal scanning laser microscope, Cytometry **14**, 105 (1993).

[18] F. Horner, M. Woerdemann, S. Muller, B. Maier, and C. Denz, Full 3D translational and rotational optical control of multiple rod-shaped bacteria, J. Biophoton. **3**, 468 (2010).

[19] A. S. Bezryadina, D. C. Preece, J. C. Chen, and Z. Chen, Optical disassembly of cellular clusters by tunable 'tug-of-war' tweezers, Light, Sci. Appl. **5**, e16158 (2016).

[20] G. Carmon, I. Fishov, and M. Feingold, Oriented imaging of 3D subcellular structures in bacterial cells using optical tweezers, Opt. Lett. **37**, 440 (2012).

[21] G. Carmon, P. Kumar, and M. Feingold, Optical tweezers assisted imaging of the Z-ring in *Escherichia coli*: measuring its radial width, New J. Phys. **16**, 013043 (2014).

[22] P. Kumar, A. Yadav, I. Fishov, and M. Feingold, Z-ring Structure and Constriction Dynamics in *E. coli*, Front. Microbiol. **8**, 1670 (2017).

[23] E. J. Peterman, F. Gittes, and C. F. Schmidt, Laser-induced heating in optical traps, Biophys. J. **84**, 1308 (2003).

[24] D. S. Weiss, J. C. Chen, J. M. Ghigo, D. Boyd, and J. Beckwith, Localization of FtsI (PBP3) to the septal ring requires its membrane anchor, the Z ring, FtsA, FtsQ, and FtsL, J. Bacteriol. **181**, 508 (1999).

[25] E. Itan, G. Carmon, A. Rabinovitch, I. Fishov, and M. Feingold, Shape of nonseptated *Escherichia coli* is asymmetric, Phys. Rev. E **77**, 061902 (2008).

[26] G. Reshes, S. Vanounou, I. Fishov, and M. Feingold, Cell shape dynamics in *Escherichia coli*, Biophys. J. **94**, 251 (2008).

[27] See Supplemental Material at http://link.aps.org/supplemental/10.1103/PhysRevE.101.062402 for a detailed description of the trap calibration, the derivation of the standard deviation of $|\alpha|$, and the error of the standard deviation and the trapping stability as a function of the trap oscillation frequency (cell II) and the trap length (cells I, III–VIII).

[28] T. L. Min, P. J. Mears, L. M. Chubiz, C. V. Rao, I. Golding, and Y. R. Chemla, High-resolution, long-term characterization of bacterial motility using optical tweezers, Nat. Methods **6**, 831 (2009).

[29] Z. Zhang, T. E. P. Kimkes, and M. Heinemann, Manipulating rod-shaped bacteria with optical tweezers, Sci. Rep. **9**, 19086 (2019).